



Published in final edited form as:

IEEE Trans Biomed Eng. 2013 July ; 60(7): 1993–2004. doi:10.1109/TBME.2013.2247603.

A Wideband Dual-Antenna Receiver for Wireless Recording From Animals Behaving in Large Arenas

Seung Bae Lee [Student Member, IEEE],

GT-Bionics Laboratory, School of Electrical and Computer Engineering, Georgia Institute of Technology, Atlanta, GA 30308 USA

Ming Yin [Member, IEEE],

School of Engineering, Brown University, Providence, RI 02912 USA

Joseph R. Manns, and

Department of Psychology, Emory University, Atlanta, GA 30322 USA

Maysam Ghovanloo [Senior Member, IEEE]

GT-Bionics Laboratory, School of Electrical and Computer Engineering, Georgia Institute of Technology, Atlanta, GA 30308 USA

Seung Bae Lee: slee87@gatech.edu; Ming Yin: ming_yin@brown.edu; Joseph R. Manns: jmanns@emory.edu; Maysam Ghovanloo: mgh@gatech.edu

Abstract

A low-noise wideband receiver (Rx) is presented for a multichannel wireless implantable neural recording (WIneR) system that utilizes time-division multiplexing of pulse width modulated (PWM) samples. The WIneR-6 Rx consists of four parts: 1) RF front end; 2) signal conditioning; 3) analog output (AO); and 4) field-programmable gate array (FPGA) back end. The RF front end receives RF-modulated neural signals in the 403–490 MHz band with a wide bandwidth of 18 MHz. The frequency-shift keying (FSK) PWM demodulator in the FPGA is a time-to-digital converter with 304 ps resolution, which converts the analog pulse width information to 16-bit digital samples. Automated frequency tracking has been implemented in the Rx to lock onto the free-running voltage-controlled oscillator in the transmitter (Tx). Two antennas and two parallel RF paths are used to increase the wireless coverage area. BCI-2000 graphical user interface has been adopted and modified to acquire, visualize, and record the recovered neural signals in real time. The AO module picks three demultiplexed channels and converts them into analog signals for direct observation on an oscilloscope. One of these signals is further amplified to generate an audio output, offering users the ability to listen to ongoing neural activity. Bench-top testing of the Rx performance with a 32-channel WIneR-6 Tx showed that the input referred noise of the entire system at a Tx–Rx distance of 1.5 m was $4.58 \mu\text{V}_{\text{rms}}$ with 8-bit resolution at 640 kSps. In an *in vivo* experiment, location-specific receptive fields of hippocampal place cells were mapped during a behavioral experiment in which a rat completed 40 laps in a large circular track. Results were compared against those acquired from the same animal and the same set of electrodes by a commercial hardwired recording system to validate the wirelessly recorded signals.

Index Terms

Behavioral neuroscience; *in vivo*; neural prosthesis; neural recording; pulse width modulation (PWM); wideband receiver

I. Introduction

Emerging technologies in bioelectronics, particularly those related to neuroprosthetic devices, have the potential to significantly improve patients' quality of life. Equally important are the tools that allow neuroscientists to conduct basic science experiments in neurophysiology research on animal models to understand the underlying principles behind operation of the nervous system, its maladies, and possible therapies, such as deep brain stimulation, for which has shown significant clinical outcomes in treatment of Parkinson's disease, tremor, and other movement disorders [1]–[3]. Another example is electrophysiological research to explore how the circuitry of the hippocampus supports memory [4]. Diseases that target the hippocampus, such as dementia and Alzheimer's, are rapidly growing in the aging industrial societies and understanding fundamentals of the healthy hippocampal memory system will be crucial for finding the causes and potential remedies for such memory disorders.

A key objective has been increasing the number of simultaneously recorded channels while minimizing damage to the neural tissue, degradation in the quality of the recorded neural signals, or biasing the natural animal behavior [5]–[12]. A related goal has been to design and develop high channel count wireless neural recording systems with potential clinical applications, such as brain–computer interfacing (BCI) for people with high level disabilities and amputees [13]–[15].

The majority of the research on wireless neural recording has so far been focused on the high density recording front ends and transmitting (Tx) side of the system, where the main challenges are miniaturization, low power consumption, and low noise to the extent that the Tx side can eventually be implanted in the animal or human body. However, in a complete wireless data acquisition system, additional components including antennas across the wireless link, external receiver (Rx), computer interface, postprocessing, data storage, and graphical user interface (GUI) should all support the Tx unit for the entire system to operate smoothly without losing information that is important for further processing of the neural signals.

Some of the major challenges in designing the Rx side are bandwidth, sensitivity, coverage of the experimental arena without leaving blind spots, and continuous streaming of the acquired data to the computer without any signal loss. In some early designs, analog samples were amplified, filtered, and directly fed into a voltage-controlled oscillator (VCO) on the Tx side to be frequency modulated (FM) after time-division multiplexing (TDM) [6]. On the Rx side, commercial FM receivers, such as the WinRadio (Melbourne, Australia) were employed. However, due to bandwidth limitation (~150 kHz) on the Rx side, such systems suffered considerable crosstalk between channels, which also limited the number of channels to less than 10. Increasing the Rx bandwidth can alleviate these problems, as demonstrated in a 32-ch wireless neural recording system by Triangle BioSystems, Inc. (Durham, NC, USA), which operates at 3.2 GHz using a custom-designed Rx with 300 MHz bandwidth [16]. Another advantage of increasing the carrier frequency is reducing the size of the optimal antennas. However, such frequencies are not useful for implantable devices due to significant absorption of high-frequency electromagnetic fields in the tissue [17].

Because of the previous limitations, most recent wireless neural recording systems have on-chip analog-to-digital converters (ADCs) on the Tx side followed by amplitude-shift keying (ASK), ON-/OFF-shift keying (OOK), frequency-shift keying (FSK), or phase-shift keying to transmit digital samples in the industrial-scientific-medical (ISM) band. The Hermes-D system, for instance, utilized an FSK scheme along with a 24-Mb/s custom-designed transceiver [18]. Rizk *et al.* used a commercial ASK/OOK transceiver at 1 Mb/s from RF Monolithics (Dallas, TX, USA) for their 96-ch system [19], while Cheney *et al.* used a commercial 2.4-GHz FSK transceiver at 1 Mb/s from Nordic Semiconductor (Trondheim, Norway) for their 16-ch system [20]. High data rate digital systems require frequency stabilization components, such as crystals and phase-locked loops (PLL), to reduce the phase noise and ensure proper synchronization between Tx and Rx, which can increase the size and power consumption of the Tx. Conversely, systems with lower data rates, encounter issues related to a limited number of channels, a low sampling rate per channel (which is not suitable for single-unit recording), or challenges associated with extensive data reduction on the Tx side [11], [21].

Using ultrawideband (UWB) transceivers is quite attractive due to their high data rate, low multipath interference, low power consumption, and relatively simple circuitry on the Tx side. Chae *et al.* developed a 128-ch neural recording system operating at 3–5 GHz band [22]. They reported a maximum data rate of 90 Mb/s; however, neither separation between Tx–Rx nor coverage of the experimental space was reported. Greenwald *et al.* also developed a 16-ch neural monitoring system with a controllable pulse rate between 90 and 270 MHz band [23]. They also illustrated the functionality of the system *in vivo*. However, 1 Mb/s of data rate is insufficient for neural recording systems with high channel count. A UWB transceiver was developed by Neuralynx (Bozeman, MT, USA) for another 128-ch system, which offered 100 Mb/s of data rate supporting up to 18-bit resolution and 32 kSps for all channels [24]. However, the architecture of the Rx was not disclosed, and it is no longer available. In general, although UWB transceivers offer many advantages, this approach is prone to interference from other RF sources. Also, due to the widespread spectrum of the carrier-less short pulses, a long synchronization time is required to achieve lossless signal acquisition and tracking on the Rx side. Moreover, complex signal processing methods are necessary to recover data in noisy environments [25].

Increasing the Tx–Rx distance for full coverage of the experimental arena regardless of the Tx position or orientation is a key requirement. Due to size limitations placed on power sources on the Tx side, this goal should ideally be achieved by consuming the least amount of power in the Tx RF block. The Tx antenna radiation pattern and its matching circuit also play a significant role. Here, the challenge is designing the most efficient and omnidirectional antenna within the limited Tx dimensions. The signal-to-noise ratio (SNR) on the Rx side may rapidly degrade to undetectable levels even at short distances if there are blind spots within the experimental arena due to multipath or high directionality of the Tx or Rx antennas. Robustness of the wireless link becomes even more important in systems with high channel count, in which low bit error rates are needed at tens of megabit per second. Constant movements of the Tx as the subject moves around the cage, resulting in the Tx antenna loading variations, and the absence of frequency stabilization components on the Tx are among other challenges.

Another key challenge that is often overlooked is the continuous, high throughput data transfer from the Rx to the computer for further processing, display, and storage in real time. For example, a 32-channel system with at least 20 kSps per channel and 16 bits/sample produces 10 Mb/s of raw data. The computer interfacing hardware and software should be designed to continuously acquire and store such data volumes in real time without any data loss or noticeable delay.

In the summary, these are the main requirements in designing the Rx side of wireless neural recording systems.

1. Compensating for size and power constraints on the Tx side, which prevent the use of complex frequency stabilization.
2. Wide bandwidth to support multiple channels without losing important neural signal information throughout the system.
3. Reliable coverage over the entire experimental arena without blind spots to compensate for movements of the Tx.
4. Robustness against interference from other RF sources.

The following two sections describe how the Tx and Rx in the sixth generation of our wireless integrated neural recording (WINEr-6) architecture address the aforementioned challenges. Section IV shows the bench-top measurement results. Section V covers the behavioral *in vivo* testing results on a rat animal model, followed by the concluding remarks.

II. WINEr-6 Transmitter Architecture

The WINEr-6 architecture is based on time-division multiplexing of pulse width modulated (TDM-PWM) signals [26]–[28]. It consists of a 32-channel wireless neural recording system on a chip on the Tx side and a custom-designed Rx, shown on the left and right sides of Fig. 1, respectively. The overall design strategy has been to reduce the complexity of the Tx unit, where size and power are extremely limited, at the cost of adding to the complexity of the Rx unit.

Following amplification and filtering of the neural signals by an array of 32 low-noise amplifiers (LNA), the outputs are combined with four monitoring signals, including half of the rectifier output voltage $V_{REC}/2$, bandgap reference V_G , a temperature-dependent voltage V_T , and V_{SS} , to be fed into the PWM block. The PWM block consists of 36 rail-to-rail comparators that compare analog inputs with a triangular waveform, similar to the analog portion of a single-slope ADC, to generate 36 PWM signals, as described in [26]–[29]. In this step that is known as analog-to-time conversion (ATC), the information stored in the analog samples is converted to pulse width, and the pulses are multiplexed by a circular shift register (CSR). The TDM-PWM signal is a pseudodigital waveform with binary levels. Thus, it is more robust against interference compared to analog signals, and it can be easily transmitted after a binary RF modulation. Hence, in this architecture, there is no need to digitize the samples on the Tx side, which can be a power- and area-consuming process at high sampling rates. Moreover, wireless transmission of a high rate serial data bit stream at tens of megabit per second requires more accurate timing and synchronization between the Tx and Rx compared to a series of TDM-PWM pulses, which width can be precisely measured by a timer on the Rx side to recover the digitized data, in a step known as time-to-digital conversion (TDC) [30].

To save power, the CSR turns ON each channel only for a short period before and during sampling. The comparator for each channel is also enabled only when that channel is being sampled. During each comparison, WINEr-6 chip is entirely quiet with no digital transition anywhere on the chip, reducing the substrate noise, pulse jitter, and dynamic power dissipation. The monitoring signals provide a unique and fairly stable pattern that can be used to indicate the beginning of each TDM-PWM frame on the Rx side, which is necessary for demultiplexing of 36 samples. Following TDM, there is a PWM masking block, which limits the minimum width of the high and low TDS-PWM pulses to ensure their accurate recovery on the Rx side.

The trimmed TDM-PWM signal drives a free-running hybrid VCO with an off-chip inductor, to be upconverted to a 428/441 MHz FSK signal. The FSK-TDM-PWM signal is then 11.4 dB amplified by a class-C RF power amplifier and transmitted by a loop antenna with 18 MHz bandwidth.

A more detailed description of the WINeR-6 Tx can be found in [27].

III. WINeR-6 Receiver and Computer Interface

Resolution of the TDM-PWM-based WINeR-6 system is determined by the accuracy of the recovered pulse width. Higher Rx bandwidth corresponds with sharper pulse edges and lower pulse width error [28]. Thus, the WINeR-6 Rx needs high enough bandwidth to receive the FSK-TDM-PWM signal while providing an adequate resolution of more than 8 bits. Most commercially available ISM-band FSK receivers only provide up to 600 kHz bandwidth [31], which is far below what is required for a neural recording system with data volume in the order of 10 Mb/s. Hence, we implemented a custom-designed Rx with 18 MHz bandwidth using commercially available off-the-shelf (COTS) components.

The WINeR-6 Rx block diagram, shown in Fig. 1(b), has four major modules in addition to the antennas: RF front end, analog signal conditioning, field-programmable gate array (FPGA) including USB 2.0 interface, and digital-to-analog converter (DAC).

A. Yagi-Uda Antenna

Like other implantable medical devices, WINeR-6 Tx has a limited power budget for RF transmission to keep its overall power consumption down. At the same time, it was desired to provide coverage over large experimental arenas in the order of $2 \times 2 \text{ m}^2$ without any blind spots. This specification required high Rx front-end sensitivity and high-gain Rx antennas. A Yagi-Uda antenna satisfies these requirements while offering wide bandwidth. Relatively high directivity of the Yagi-Uda antenna was mitigated by the inclusion of two antennas in each WINeR-6 Rx. We designed a three-element Yagi-Uda antenna based on [32], as shown in Fig. 2.

B. RF Front End

In order to increase the wireless coverage of the experimental arena and eliminate blind spots, the Rx was equipped with two identical RF front ends, each with its own antenna. As shown in Fig. 1, the FSK-TDM-PWM signal from the Tx was picked up by each antenna, and amplified/filtered independently through its parallel RF front end. Each path has an RF power detector (ADL5513), and depending on the strength of the received RF signal from each path, an RF switch connects the stronger one to the mixer. Depending on the size of the experimental arena, the wireless coverage can potentially be extended even further by increasing the number of antennas and parallel RF front-end paths.

Each RF front end consists of an RF-LNA (MAX2640) with a gain and noise figure of 15.1 and 0.7 dB at 400 MHz, respectively, followed by a gain stage (BGA2712) that provides an additional 24 dB amplification. The RF front end can provide up to 1.5 GHz bandwidth, while two passive third-order Cheby-shev bandpass filters with 403–490 MHz bandwidth are placed before and after the gain stage to provide selectivity around the Tx signal and limit the out-of-band noise. The RF front end thus provides 45 dB gain and 87 MHz bandwidth.

C. Analog Signal Conditioning

The amplified and filtered FSK signal is fed into a mixer, which is a 50 MHz to 1 GHz quadrature demodulator with 75 MHz bandwidth (AD8348). The mixer has a built-in variable gain amplifier (VGA) that provides -18.5 to $+25.5$ dB programmable gain. The VGA output drives two (I and Q) double-balanced Gilbert cell down-conversion mixers, which down convert the RF signal to 43.5/56.5 MHz IF band. The IF-TDM-PWM signal is then further filtered and amplified in the baseband. To create a tunable local oscillator (LO) for the down converter, we have utilized a 720–1750 MHz VCO (V585ME41-LF) from Z-Comm (San Diego, CA, USA). The LO frequency is divided by two inside the mixer, resulting in its ability to receive RF frequencies in 360–875 MHz range.

IF amplifiers and filters improve the SNR by eliminating the out-of-band interference. AD4899-1 amplifier was chosen for this block because of its 300 MHz unity gain bandwidth, ultralow distortion, and low noise. Three instances of this amplifier have been implemented with a total IF gain of 46 dB. In order to reject all adjacent channels' interference, a bandpass filter (KR2850) from KR Electronics (Avenel, NJ, USA) has been included between the second and the third amplifiers. The filter has an 18 MHz bandwidth from 41–59 MHz and a 1 dB pass-band ripple.

The amplified and filtered IF-FSK signal is fed into a logarithmic limiting IF amplifier (AD8309) and a high speed comparator (TLV3501) with 4.5 ns delay. This stage recovers the rail-to-rail baseband FSK-TDM-PWM signal, which is then fed into an FPGA to be FM demodulated in the digital domain to recover the TDM-PWM signal.

D. FPGA Module

We used a COTS FPGA module, called Xylo-EM [33], which includes an Altera FPGA (EP2C5T144C8), 2 MB of synchronous dynamic random access memory (SDRAM) for data buffering, and the USB interface circuitry.

1) FSK Demodulation via TDC—A TDC in the FPGA demodulates the down-converted IF-FSK signal in the digital domain. The FPGA-based TDC block diagram is shown in Fig. 3. The IF-FSK signal is used as the clock signal for the 8-bit encoder and D-type flip-flops in the delay chain. A unit gate delay τ is the average time required for a rising or falling edge to propagate through a four-input AND gate. As a falling edge of the IF-FSK propagates through the chain of AND gates, the following rising edge saves a snapshot of the AND gate outputs in the rising edge-triggered D flip-flop register. Since the duration of a logic low is different in two FSK cycles at two different frequencies, the contents of the D flip-flop register at every rising edge of the IF-FSK can determine the period of that FSK half-cycle, ΔT . The 8-bit encoder then converts the contents of the D flip-flop register to an 8-bit value, $C1[7:0] = \Delta T/\tau$. The measured FSK pulse widths are accumulated in two separate registers, PWH and PWL, after comparing C1 with a programmable threshold value that discriminates between the two periods in the IF-FSK. The two frequencies in the IF-FSK are 43.5 and 56.5 MHz, which correspond to ΔT of 11.5 and 8.8 ns, respectively. Considering $\tau = 304$ ps in this FPGA, $\Delta T/\tau$ yields 38 and 29 delay cells for the low- and high-frequency half-cycles, respectively. To distinguish between these values, their average, 34, was used for as the FSK period threshold.

Although the absolute values of PWH and PWL vary with the instantaneous changes in the triangular waveform, the TDM-PWM duty cycle is relatively more stable and changes mainly with amplitude of the analog sample [28]. Thus, $C2[14:0]$ was calculated inside the FPGA from $PWH/(PWH + PWL)$ of the recovered TDM-PWM signal as a normalized value within 0 and 1 that is proportional to the analog sample. C2 passes through a noise filtering

block, which removes the pulse widths that are too small or too large to eliminate sharp glitches. The demultiplexing block that follows is designed to detect the marker created from four monitoring signals ($V_{REC}/2$, V_{BG} , V_T , and V_{SS}), which indicates the beginning of each TDM-PWM pulse frame. The pulse width following the monitoring signals is the sample taken from the first neural recording channel. In order to mark this channel for the BCI-2000, running on the computer, the demultiplexing block adds a flag to C3[14:0] as its most significant bit (MSB) such that the MSB of the 16 bits digitized output, C4[15:0], would be “1” for the first channel and “0” for all other channels.

2) Automatic Frequency Tracking (AFT)—Frequency stabilization components, such as PLL or crystals, were not used in the WINeR-6 Tx to reduce its size and power consumption [27]. As a result, the Tx carrier frequency varies with temperature, supply voltage, and to a lesser extent antenna loading variations. To compensate for these variations, digital AFT function was implemented in the Rx. Following TDC, the AFT block averages 500 IF-FSK periods, which are available from C1[7:0]. The AFT tries to match the low-pass-filtered carrier period from TDC with a programmable reference period by changing the LO control voltage via a DAC. The AFT changes the LO frequency until the down-converted IF-FSK spectrum is centered at 50 MHz.

3) Continuous High-Throughput USB Interface—A USB 2.0 interface delivers a continuous stream of digitized neural data from WINeR-6 Rx to the computer in real time. A high-speed EZ-USB chip (Cy7C68013A) was chosen for its high throughput, programmability, reliability, and ease of use. The data rate in the 32-ch WINeR-6 system is in the order of 10 Mb/s for 640 kSps. When USB operates in the burst mode, the delays between successive USB data packets in the computer are quite unpredictable, varying from 100 μ s to a few ms. To ensure continuous real-time recording without data loss, we have used a 2 MB SDRAM between the TDC and the USB interface blocks to buffer the incoming data. The EZ-USB chip is set to operate in the slave-FIFO mode, controlled by a master module implemented in the Altera FPGA. The USB control module in the FPGA manages data transfers between the SDRAM and USB. It writes the 16-bit data created in the TDC module into the SDRAM at the falling edge of every TDM-PWM pulse. In this module, the EZ-USB reads a 16-bit sample from the SDRAM into its internal 2056 Byte FIFO. Meanwhile, the EZ-USB chip continuously checks its own FIFO state, and when it is full, commits the data to the computer.

E. DAC Module

To assist users with visualizing and determining the quality of the incoming neural signals and to be compatible with some commercial hardwired neural recording back ends, WINeR-6 Rx includes a four-channel 16-bit DAC (AD5664R), which operates at 71.1 kSps. The clock, data, and enable signals for the DAC are generated by the same FPGA, which also allows users to select 3 out of 32 digitized and demultiplexed neural recording channels as inputs to the DAC. The DAC converts them into three analog signals that can be accessed independently through SMA connectors. In addition, one of these three analog signals can be selected and used to drive a 1-W audio amplifier with dc volume control (TDA7052A). The output of the audio amplifier drives an 8 Ω speaker, allowing users to identify the spike activity by how it sounds. The first channel of the DAC is used in the AFC block, described in Section III-D.3.

F. GUI

BCI-2000, an open-source piece of software for BCI research applications, displays the received neural signals on the GUI and saves them on the computer hard disk in real time [34]. It consists of four modules that communicate within each other, as shown in Fig. 4(a).

The “source” module receives data from the data acquisition device (WINEr-6 Rx), saves it, and sends it to the signal processing module. The “application” module is responsible for visualization on the computer screen. We have modified the source module to continuously receive the neural data from WINEr-6 Rx through the USB port.

Fig. 4(b) shows the flowchart for data acquisition algorithm in the source module, which performs two important tasks. First, it detects the marker that indicates sampled data for the first channel and time-division demultiplexes the rest of the incoming data accordingly. While the program is running, the module waits for a predefined amount of data to arrive by saving it in a temporary memory space before arranging the samples. Second, the source module applies a simple postprocessing algorithm to compensate for some of the nonlinear characteristics of the ATC process on the Tx side. The triangular waveform generator (TWG) block in particular has nonlinear characteristics that can degrade the quality of the TDM-PWM signal. In a one-time calibration process, the nonlinear characteristics of the TWG block in each WINEr-6 ASIC can be measured and stored in the BCI-2000 to be applied to the incoming data from that ASIC before further signal processing.

The source module also receives a state vector from the “application” module and saves it in a file in *.dat format together with the organized raw data. The signal processing module is responsible for a wide range of functions from various filters to spike detection, classification, and information extraction, desired by the user, which are out of the scope of this paper. It will pass on anything that needs to be visualized on the GUI to the application module, which also visualizes the received neural signals on the computer screen, and generates the state vector to be fed back to the source module. In this way, the BCI-2000 software shows neural signals on the computer screen and saves them on the hard disk in real time.

IV. Bench-Top Measurement Results

The RF, analog, and DAC modules of WINEr-6 Rx were implemented on separate custom-designed printed circuit boards for electromagnetic isolation and shielding, as shown in Fig. 5. They are carefully fitted in a $17.9 \times 17.5 \times 7.6 \text{ cm}^3$ aluminum enclosure along with the COTS FPGA module and SMA interconnects. The WINEr-6 Rx consumes 80 and 290 mA from -5 and 5 V supplies, respectively. The FPGA module is powered from the USB port. It has on-board 3.3 and 5 V regulators, which also power the DAC module.

A. Antennas

The WINEr-6 Rx was bench-top tested along with the three-element Yagi-Uda antennas, designed based on specifications in Fig. 2. Fig. 6(a) shows the measured return loss of the antennas. Considering the effect of baluns, the 10 dB return loss of the fabricated antennas shows 54 MHz bandwidth, over the $424\text{--}478 \text{ MHz}$ frequency range.

A loop antenna ($3.5 \times 2 \text{ cm}^2$) was designed for the WINEr-6 Tx, as shown in the lower right panel in Fig. 5 [35]. The vertical and horizontal radiation patterns of the WINEr-6 Tx are shown in Fig. 6(b), which were measured in an outdoor open space to minimize external interference. The WINEr-6 Tx was placed in the center of the measurement area, and the received signal strength from the Yagi-Uda Rx antenna was measured at 1 m distance from the Tx. The Tx was manually rotated clockwise from 0° to 360° with 10° increments. Fig. 6(b) shows that the WINEr-6 Tx antenna has maximum signal variation of 25 dB .

B. RF Front End

The S_{11} and S_{21} of the RF front end have been measured and depicted in Fig. 7. The total RF gain for this block was 45 dB over 403–490 MHz range, which is matching in the center and slightly wider than the Yagi–Uda Rx antenna bandwidth.

C. Complete WINeR-6 Tx–Rx Operation

To test the entire WINeR-6 system (see Fig. 1) operation in a bench-top setting, an artificial spike waveform was played from a DAC (MP3 player), attenuated to 1 mV peak amplitude, and applied to all 32 input channels. The input signal was then amplified and filtered by the LNA block with 67.8 dB gain and 1 Hz – 8 kHz bandwidth. The TWG output signal was adjusted at ± 1.4 V and 640 kHz, setting the overall sampling rate of the WINeR-6 system. The TDM-PWM block compared the 32 LNA outputs and 4 monitoring signals with the TWG output, and the MUX organized the resulting PWM samples into frames of 36 pulses. In order to make sure that the TDM-PWM pulses were detectable on the Rx side, i.e., they were neither too narrow nor too wide, when the input was below -1.1 V or above 1.3 V, the ATC pulse width was kept constant by the PWM mask. This signal drove the on-chip MOS varactor of the hybrid LC-VCO, running at 428/441 MHz in the FSK mode.

The transmitted FSK-TDM-PWM carrier was picked up 1.5 m away from the WINeR-6 Tx by the Rx antenna. In the FPGA, the down-converted signal was FSK demodulated and digitized via TDC to 16-bit samples, which were buffered in the SDRAM and delivered to a computer through its USB port. Three out of the 36 channels were further converted to analog signals in the DAC module. The upper and lower traces in Fig. 8 are the LNA output on the Tx side and the corresponding DAC output on the Rx side for the same channel, respectively. The measured WINeR-6 latency from the LNA output of the Tx to the Rx DAC output was ~ 1 μ s.

Using the previous setup and bypassing the LNA block, the integral nonlinearity (INL) and differential nonlinearity (DNL) of the rest of WINeR-6 were measured as a wireless data acquisition system, combining ATC and TDC on the Tx and Rx sides, respectively. In this measurement, a constant voltage, generated by an Agilent 33250A function generator with 12-bit resolution was applied to the LNA output of ch-12. By varying the dc input from rail to rail, ± 1.5 V, the increments in the 16-bit digitized value from the same channel were recorded on the Rx side, which was located 1.5 m from the Tx. Considering the PWM mask, a window between -1.1 and 1.3 V was selected to measure the DNL and INL, and the LSB size was set to 9.4 mV for 8 bit resolution. Fig. 9 shows the measured DNL and INL for the WINeR-6 prototype, which were within $(-0.364, +0.444)$ LSB and $(-0.468, +0.226)$ LSB, respectively.

In addition to the INL and DNL, a tone test was conducted by applying a 600 Hz sinusoidal waveform to ch-12 LNA output. The test results in Fig. 10 show a spurious-free dynamic range (SFDR) of 64.95 dB with a hardwired link. With a wireless link at 150 cm Tx–Rx separation, the SFDR was 58.86 dB. This measurement indicates that linearity performance of WINeR-6 has decreased by 6.1 dB because of the 150 cm wireless link.

D. WINeR-6 Noise Performance

To analyze the noise contribution from different WINeR-6 blocks, noise measurement was performed in an unshielded laboratory environment in several configurations shown in Fig. 11. In each case, we applied a fast Fourier transform on 20 s of the recorded signal in the computer to derive its spectrum and refer it back to the input. Fig. 11(a) shows the TDC noise measurement setup. Here, a series of pulses with 50% duty cycle were generated by a function generator and fed into the TDC block in the FPGA. We expected the TDC noise to

be very small, but it should be noted that the measurement included the function generator phase noise as well, which was considered negligible. In Fig. 11(b), the LNA outputs are forced to ground to cancel the LNA noise. Noise of the wireless link has also been bypassed by directly connecting the TDM-PWM signal from Tx to the TDC input on the Rx side through a high-speed digital isolator (ISO721). The setup in Fig. 11(c) is similar to the one in Fig. 11(b) except for the fact that the LNA noise has been included by grounding the LNA inputs. Finally, Fig. 11(d) shows the noise measurement setup for the entire WINeR-6 system. In all noise measurements, the LNA bandwidth was set to 200 Hz to 8 kHz, while the input referred noise was integrated over a wider range from 1 Hz to 10 kHz.

Using the setup in Fig. 11(d) (i.e. the entire system), we swept the Tx–Rx distance from 30 to 210 cm to observe the effect of Tx–Rx separation on the noise of the wireless link without shielding. The input referred noise amplitudes for these measurements are shown in Figs. 12 and 13. According to these graphs and our theoretical analysis in [28], the noise from the wireless Rx is obviously the dominant noise source for the current 32-ch WINeR-6 system prototype, especially at large Tx–Rx separation. At the nominal Tx–Rx distance of 1.5 m, the effective number of bits is 8 bits considering the INL and DNL measurements in Fig. 9. In addition, the measured Rx sensitivity was -65 dBm. Table I summarizes the key measured specifications of the entire WINeR-6 system.

V. *In Vivo* Experimental Results

To further evaluate the performance of the WINeR-6 system, we compared its overall performance to that of a commercial hardwired system, based on NSpike [36], in a meaningful behavioral neuroscience experiment, in which action potentials were recorded from hippocampal pyramidal neurons of a rat as it completed laps on a relatively large circular track (~ 1 m²). The subject was a 15-month-old male Long-Evans rat, weighing approximately 550 g. This set of experiments was conducted with approvals from the Institutional Animal Care and Use Committees at the Georgia Institute of Technology and Emory University.

The rat was implanted with a chronic recording assembly that contained 32 tetrodes (bundle of four electrodes) targeted at the dorsal hippocampus. Further details can be found in [37] and [38]. The electrodes were connected to four 36-pin male Nanoconnectors from Omnetics (Minneapolis, MN, USA). In each of the four connectors, four lateral pins were used for grounding and reference, and the other 32 were connected to 8 out of 32 tetrodes. The WINeR-6 analog front-end bandwidth for this experiment was set to 400 Hz–8 kHz with a total gain of 8000 for recording single-neuron action potentials, similar to the settings for the NSpike system. The experiment was carried out in a circular track with an outer diameter of 91.4 cm and width of 7.6 cm, as shown in Fig. 14, which was setup in a small shielded cubicle. During the test, the rat completed two sessions of 40 laps each, in which video and neural data were recorded with both systems. The rat was rewarded for completing each lap with a small piece of chocolate.

To provide sufficient wireless coverage, four antennas from two WINeR-6 receivers were mounted on stands made of PVC pipes, and positioned roughly at 3, 6, 9, and 12 o'clock slightly above the circular track in order not to miss any neural signal during the experiment due to fading. The two WINeR-6 Rxs and associated computers were placed outside the cubicle.

Fig. 15 shows the operating diagram of the dual-Rx solution. When two receivers record the same neural signals from a single WINeR-6 Tx, the data need to be synchronized by indicating the same marker signals in both recorded data streams. For this purpose, a predefined marker was generated in the master FPGA when a push button was pressed. This

marker signal was then transferred to the master BCI-2000, and easily distinguished from the digitized neural signals. A similar marker signal was generated in the slave FPGA at the same time and sent to the slave BCI-2000. Fig. 16 shows a snapshot of 32 neural recording channels which was shown in real time on one of the two BCI-2000 GUIs. A similar WINeR-6 configuration could be used to simultaneously record neural signals from multiple animal subjects in the same experimental arena in a socially relevant context, provided that their Tx–Rx pairs were tuned at different center frequencies.

The exact same experiment was repeated with the same animal and the same electrode positions using the hardwired NSpike system, for which sampling rate, gain, and bandwidth were adjusted to be very close to that of the WINeR-6 system. A video camera was mounted above the track to record the rat position in synchrony with the neural recording. The video frames were synchronized with the neural data from WINeR-6 by flashing the LED, shown in Fig. 15, as an optical cue.

After completion of the data recording phase, spike classification was conducted on both wireless and hardwired datasets using the Offline Sorter software from Plexon (Dallas, TX, USA) in order to isolate activity from individual neurons. Fig. 17(a) and (b) shows spike waveforms across four channels (wires) of the same tetrode, activity from what was thought to be the same pyramidal neuron recorded during the WINeR-6 (wireless) and NSpike (hardwired) sessions, respectively. After classifying putative single neurons, the spike firing location for the best isolated units were marked on the circular track by synchronizing the timing of the spiking activity with the rat location on the recorded video data.

Many pyramidal neurons in the dorsal rat hippocampus, termed place cells, show location-specific activity, and the location at which the greatest firing rate of an individual neuron occurs is often referred to as its place field [39]. Fig. 18 shows a place field plot for a place-cell recorded during both recording sessions. Brighter colors indicate a higher firing rate, and gray colors show the overlapping trajectories of the rat as it completed laps on the circular track. Based on the similar spatial selectivity of the place fields in both plots and similar firing rates, the results suggest that the WINeR-6 wirelessly recorded data are similar to that of the hardwired recording setup (gold standard) in an experiment with a rat freely behaving in a 1-m² arena. The results illustrate the feasibility of the WINeR-6 system as a substitute for hardwired systems in behavioral neuroscience experiments. The lower SNR of the WINeR-6 system, which is also noticeable in Fig. 17 classified single- neuron waveforms, has resulted in lower concentration of the place cell firing around the peak in Fig. 18.

VI. Conclusion

We have presented a complete high performance multichannel WINeR system with emphasis on the Rx side. WINeR-6 architecture offers 18 MHz RF bandwidth and high data throughput all the way from the neural tissue to the computer for real-time electrical, visual, and acoustic representation of 32 simultaneously recorded channels. A significant feature of the WINeR-6 system, which has been demonstrated in a real behavioral neuroscience experiment on an awake freely behaving small animal subject (rat), is its ability to provide wireless coverage over a large experimental arena (>1 m²) without losing data or leaving any blind spots, while keeping the Tx power consumption, the SNR, and resolution of the entire system at a reasonable level. Utilization of the TDM-PWM method to simplify the Tx, multiple custom-designed high gain antennas, automatic Tx carrier frequency tracking, high-resolution FPGA-based FSK demodulation, and TDC are some of the techniques that have significantly improved WINeR-6 performance compared to systems with similar complexity and power consumption. We are now working to further improve the WINeR system

resolution, noise performance, and power consumption to be wirelessly powered inside a smart experimental arena, known as the EnerCage [27], [40].

Acknowledgments

This work was supported in part by the National Institute of Health, NINDS Grant 1R01NS062031-01A1, and the National Science Foundation under Award ECCS-824199.

The authors would like to thank F. Getaneh in the Manns lab and several members of the GT-Bionics lab for their assistance with the animal experiments.

References

- Breit S, Schulz JB, Benabid AL. Deep brain stimulation. *Cell Tissue Res.* Aug.2004 318:275–288. [PubMed: 15322914]
- Holtzheimer PE, Mayberg HS. Deep brain stimulation for psychiatric disorders. *Ann Rev Neurosci.* 2011; 34:289–307. [PubMed: 21692660]
- Wichmann T, DeLong MR. Deep brain stimulation for neurologic and neuropsychiatric disorders. *Neuron.* Oct; 2006 52(1):197–204. [PubMed: 17015236]
- Manns JR, Eichenbaum H. Evolution of declarative memory. *Hippocampus.* Sep; 2006 16(9):795–808. [PubMed: 16881079]
- Johannessen EA, Wang L, Cui L, Tang TB, Ahmadian M, Astaras A, Reid SWJ, Yam PS, Murray AF, Flynn BW, Beaumont SP, Cumming DRS, Cooper JM. Implementation of multichannel sensors for remote biomedical measurements in a microsystems format. *IEEE Trans Biomed Eng.* Mar; 2004 51(3):525–535. [PubMed: 15000383]
- Mohseni P, Najafi K, Eliades SJ, Wang X. Wireless multichannel biopotential recording using an integrated FM telemetry circuit. *IEEE Trans Neural Syst Rehabil Eng.* Sep; 2005 13(3):263–271. [PubMed: 16200750]
- Sawan M, Hu Y, Coulombe J. Wireless smart implants dedicated to multichannel monitoring and microstimulation. *IEEE Circuits Syst Mag.* 2005; 5(1):21–39.
- Harrison RR, Watkins PT, Kier RJ, Lovejoy RO, Black DJ, Greger B, Solzbacher F. A low-power integrated circuit for a wireless 100-electrode neural recording system. *IEEE J Solid-State Circuits.* Jan; 2007 42(1):123–133.
- Sodagar AM, Wise KD, Najafi K. A fully integrated mixed-signal neural processor for implantable multichannel cortical recording. *IEEE Trans Biomed Eng.* Jun; 2007 54(6):1075–1088. [PubMed: 17554826]
- Peng CC, Zhiming X, Bashirullah R. Toward energy efficient neural interface. *IEEE Trans Biomed Eng.* Nov; 2009 56(11):2697–2700. [PubMed: 19709960]
- Farshchi S, Pesterev A, Nuyujukian P, Guenterberg E, Mody I, Judy JW. Embedded neural recording with tinyOS-based wireless-enabled processor modules. *IEEE Trans Neural Syst Rehabil Eng.* Apr; 2010 18(2):134–141. [PubMed: 20071270]
- Gosselin B. Recent advances in neural recording microsystems. *Sensors.* Apr.2011 11:4572–4597. [PubMed: 22163863]
- Nurmikko AV, Donoghue JP, Hochberg LR, Patterson WR, Song YK, Bull CW, Borton DA, Laiwalla F, Park S, Yin M, Aceros J. Listening to brain microcircuits for interfacing with external world—Progress in wireless implantable microelectronic neuroengineering devices. *Proc IEEE.* Mar; 2010 98(3):375–388.
- Lebedev MA, Nicolelis MAL. Brain–machine interfaces: Past, present and future. *Trends Neurosci.* Jul; 2006 29(9):536–546. [PubMed: 16859758]
- Hochberg LR, Donoghue JP. Sensors for brain computer interfaces. *IEEE Eng Med Biol Mag.* Sep; 2006 25(5):32–38. [PubMed: 17020197]
- Fan D, Rich D, Holtzman T, Ruther P, Dalley JW, Lopez A, Rossi MA, Barter JW, Salas-Meza D, Herwik S, Holzhammer T, Morizio J, Yin HH. A wireless multichannel recording system for freely behaving mice and rats. *PLoS ONE Neurosci.* Jul.2011 6(7)10.1371/journal.pone.0022033

17. Poon AY, O'Driscoll S, Meng TH. Optimal frequency for wireless power transmission into dispersive tissue. *IEEE Trans Antennas Propag.* May; 2010 58(5):1739–1750.
18. Miranda H, Gilja V, Chestek CA, Shenoy KV, Meng TH. HermesD: A high-rate long-range wireless transmission system for simultaneous multichannel neural recording applications. *IEEE Trans Biomed Circuits Syst.* Jun; 2010 4(3):181–191. [PubMed: 23853342]
19. Rizk M, Obeid I, Callender SH, Wolf PD. A single-chip signal processing and telemetry engine for an implantable 96-channel neural data acquisition system. *J Neural Eng.* Jun.2007 4:309–21. [PubMed: 17873433]
20. Cheney D, Goh A, Xu J, Gugel K, Harris JG, Sanchez JC, Principe JC. Wireless, in vivo neural recording using a custom integrated bioamplifier and the pico system,” in. *Proc 3rd IEEE Int Eng Med Biol Soc Conf Neural Eng.* Mar.2007 :19–22.
21. Zhang F, Aghagolzadeh M, Oweiss K. A fully implantable, programmable and multimodal neuroprocessor for wireless, cortically controlled brain-machine interface applications. *J Signal Process Syst.* Mar.2012 69:351–361. [PubMed: 23050029]
22. Chae M, Yang Z, Yuce MR, Hoang L, Liu W. A 128-channel 6 mW wireless neural recording IC with spike feature extraction and UWB transmitter. *IEEE Trans Neural Syst Rehabil Eng.* Aug; 2009 17(4):312–321. [PubMed: 19435684]
23. Greenwald E, Mollazadeh M, Hu C, Tang W, Culurciello E, Thakor NV. A VLSI neural monitoring system with ultra-wideband telemetry for awake behaving subjects. *IEEE Trans Biomed Circuits Syst.* Apr; 2011 5(2):112–119. [PubMed: 23851199]
24. Neuralynx Corp; Bozeman, MT, USA; [Online]. Available: <http://www.neuralynx.com>
25. Mercier PP, Bhardwaj M, Daly DC, Chandrakasan AP. A low-voltage energy-sampling IR-UWB digital baseband employing quadratic correlation. *IEEE J Solid-State Circuits.* Jun; 2010 45(6):1209–1219.
26. Yin M, Ghovanloo M. A low-noise clockless simultaneous 32-channel wireless neural recording system with adjustable resolution. *Analog Integrated Circuits and Signal Process.* Mar; 2011 66(3):417–431.
27. Lee SB, Lee H, Kiani M, Jow U, Ghovanloo M. An inductively powered scalable 32-channel wireless neural recording system-on-a-chip for neuroscience applications. *IEEE Trans Biomed Circuits Syst.* Dec; 2010 4(6):360–371. [PubMed: 23850753]
28. Yin M, Ghovanloo M. Using pulse width modulation for wireless transmission of neural signals in multichannel neural recording systems. *IEEE Trans Neural Syst Rehabil Eng.* Aug; 2009 17(4):354–363. [PubMed: 19497823]
29. Baker, RJ. *CMOS Circuit Design, Layout, and Simulation.* 3. Hoboken, NJ, USA: Wiley; 2010.
30. Kalisz J, Szplet R, Poniecki A. Field programmable gate array based time-to-digital converter with 200-ps resolution. *IEEE Trans Instrum Meas.* Feb; 1997 46(1):51–55.
31. Analog Devices, ADF7025, High Performance ISM-Band Transceiver IC. [Online]. Available: http://www.analog.com/static/imported-files/data_sheets/ADF7025.pdf
32. Milligan, TA. *Modern Antenna Design.* 2. Hoboken, NJ, USA: Wiley; 2005.
33. FX2 FPGA & ARM Boards, KNJN LLC. [Online]. Available: <http://www.knjin.com/FPGA-FX2.html>
34. BCI-2000 Homepage. [Online]. Available: <http://www.bci2000.org>
35. Nordic Semiconductor, nAN900—05 nRF9E5 RF and Antenna Layout. [Online]. Available: http://www.nordicsemi.com/eng/content/download/2449/29496/file/nAN900-05_nRF9E5_RF_and_antenna_layout_rev2_1.pdf
36. NSpike. [Online]. Available: <http://nspike.sourceforge.net/>
37. Komorowski RW, Manns JR, Eichenbaum H. Robust conjunctive item-place coding by hippocampal neurons parallels learning what happens where. *J Neurosci.* Aug; 2009 29(31):9918–9929. [PubMed: 19657042]
38. Manns JR, Eichenbaum H. A cognitive map for object memory in the hippocampus. *Learning Memory.* Sep; 2009 16(10):616–624. [PubMed: 19794187]
39. O'Keefe J. Place units in the hippocampus of the freely moving rat. *Exp Neurol.* Apr; 1976 51(1):78–109. [PubMed: 1261644]

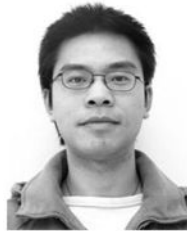
40. Jow U, Kiani M, Huo X, Ghovanloo M. Towards a smart experimental arena for long-term electrophysiology experiments. *IEEE Trans Biomed Circuits Syst.* Oct; 2012 6(5):414–423. [PubMed: 23853228]

Biographies



Seung Bae Lee (S'08) received the B.S. degree in electrical engineering from Hanyang University, Seoul, Korea, in 2007 and the M.S. degree in electrical and computer engineering from the Georgia Institute of Technology, Atlanta, GA, USA, in 2010. He is currently working toward the Ph.D. degree at the Georgia Institute of Technology.

He came to Georgia Tech in August 2007 and joined GT-Bionics Laboratory in May 2008. His current research interest includes an ultralow power RF receiver for biomedical and wearable applications as well as a wireless neural recording system.



Ming Yin (S'06–M'10) received the B.S. and M.S. degrees in electronics engineering from Tsinghua University, Beijing, China, and the Ph.D. degree in electrical engineering from North Carolina State University, Raleigh, NC, USA.

He is currently a Postdoctoral Fellow at Brown University, Providence, RI, USA, working on a wireless neural recording system. His research interests include low noise, low power analog/mixed circuit design for wireless biomedical applications.



Joseph R. Manns received the Ph.D. degree in psychology from the University of California, San Diego, San Diego, CA, USA, in 2002.

After completing a postdoctoral fellowship at Boston University in 2007, he joined the faculty at Emory University, Atlanta, GA, USA, where he is currently an Assistant Professor in the Department of Psychology.

Dr. Manns received the postdoctoral Ruth L. Kirschstein National Research Service Award (2003–2006) and the Pathway to Independence Award (K99/R00; 2006–2011) by the National Institutes of Health.



Maysam Ghovanloo (S'00–M'04–SM'10) was born in Tehran, Iran, in 1973. He received the B.S. degree in electrical engineering from the University of Tehran, Tehran, in 1994, the M.S. degree in biomedical engineering from the Amirkabir University of Technology, Tehran, in 1997, and the M.S. and Ph.D. degrees in electrical engineering from the University of Michigan, Ann Arbor, MI, USA, in 2003 and 2004, respectively.

From 2004 to 2007, he was an Assistant Professor in the Department of Electrical and Computer Engineering, North Carolina State University, Raleigh, NC, USA. In June 2007, he joined the faculty of Georgia Institute of Technology, Atlanta, GA, USA, where he is currently an Associate Professor and the Founding Director of the GT-Bionics Laboratory at the School of Electrical and Computer Engineering. He has authored or coauthored more than 100 peer-reviewed conference and journal publications.

Dr. Ghovanloo is an Associate Editor of the IEEE Transactions on Biomedical Engineering, IEEE Transactions on Biomedical Circuits and Systems, and a member of the Imagers, MEMS, Medical, and Displays subcommittee at the International Solid-State Circuits Conference. He also served on the editorial board for the IEEE Transactions on Circuits and Systems, PART-II from 2007 to 2011. He received the 2010 CAREER Award from the National Science Foundation. He received the Tommy Nobis Barrier Breaker Award for Innovation and the Distinguished Young Scholar Award from the Association of Professors and Scholars of Iranian Heritage. He has organized several special sessions and was a member of Technical Review Committees for major conferences in the areas of circuits, systems, sensors, and biomedical engineering. He is a member of the Tau Beta Pi, AAAS, Sigma Xi, IEEE Solid-State Circuits Society, IEEE Circuits and Systems Society, and IEEE Engineering in Medicine and Biology Society.

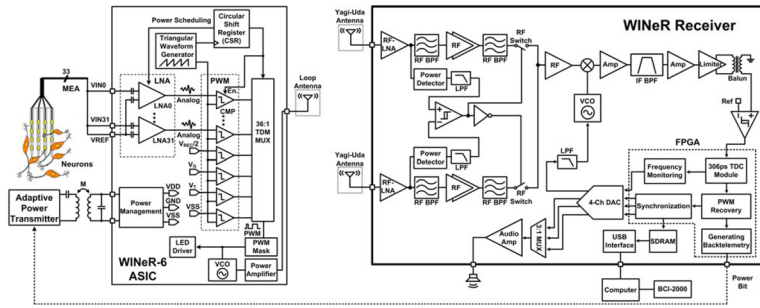


Fig. 1. Block diagram of the entire wireless implantable neural recording (WIneR-6) system: Tx (left) and Rx (right).

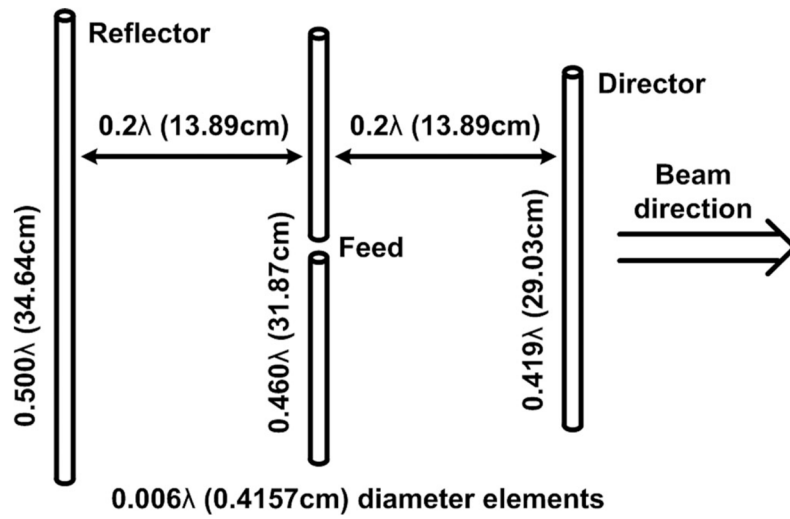


Fig. 2.
Three-element Yagi-Uda dipole antenna designed for 433 MHz carrier.

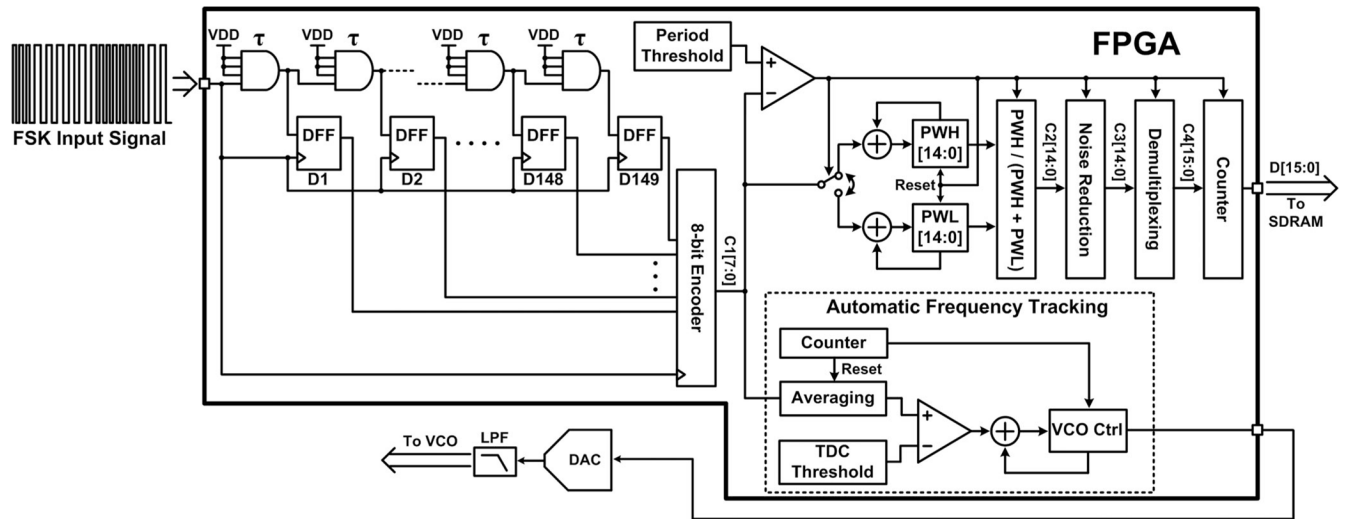


Fig. 3. FPGA-based high-resolution TDC, using a delay cell chain with $\tau = 304$ ps and an AFT block.

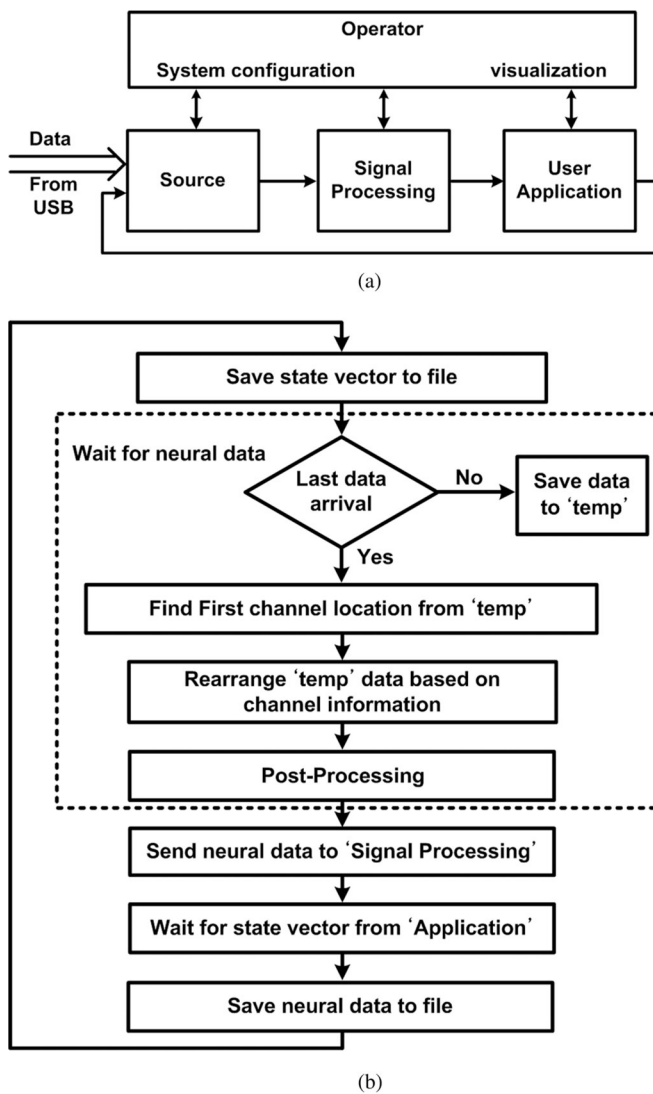


Fig. 4. (a) Core modules and their interactions in the BCI-2000. (b) Data acquisition flowchart of the "Source" module.

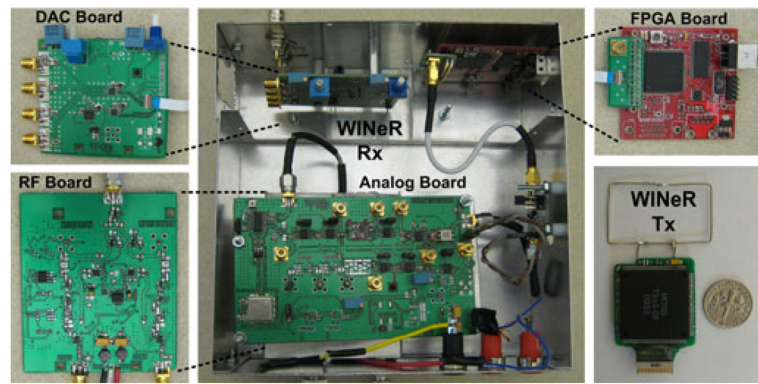
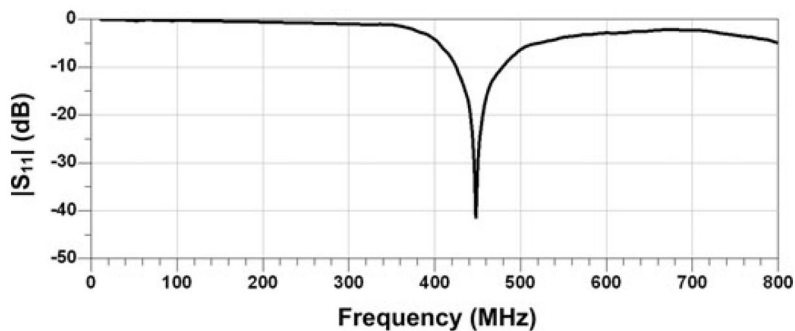
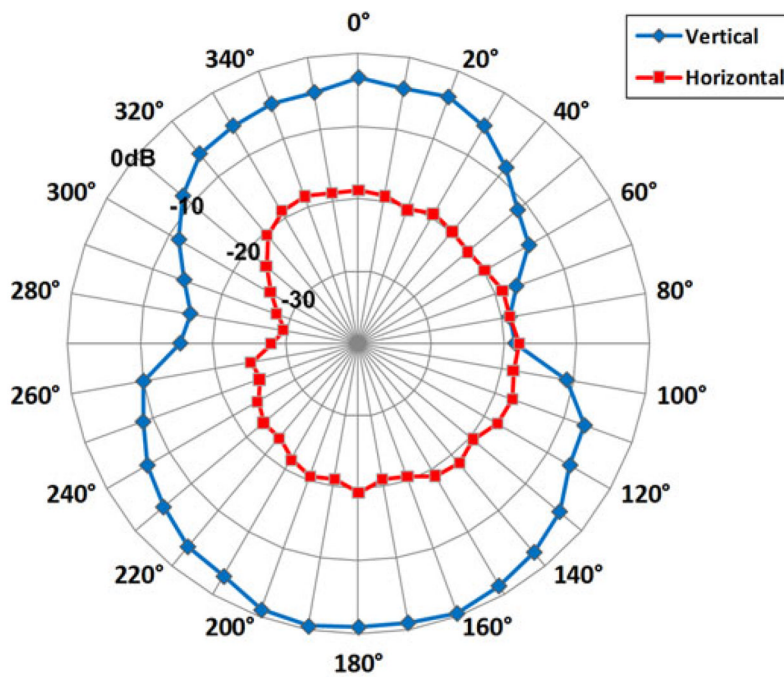


Fig. 5.
WINEr-6 Rx and Tx hardware components.



(a)



(b)

Fig. 6. (a) Measured return loss of the Rx Yagi-Uda antenna. The -10 dB bandwidth was 54 MHz from 424 to 478 MHz frequency range. (b) Relative radiation patterns of WINEr-6 Tx at 433 MHz measured by the Rx antenna.

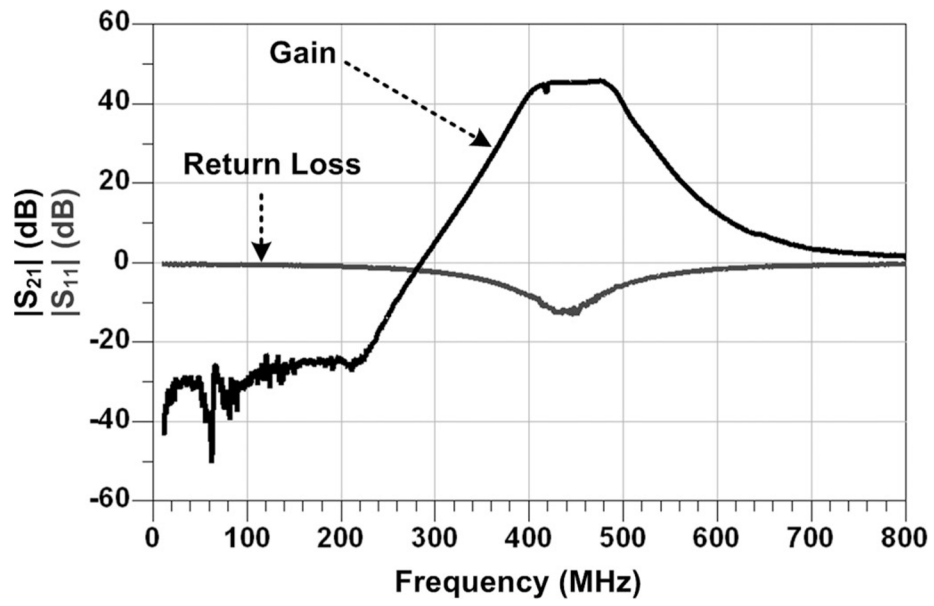


Fig. 7.
Measured return loss and gain of the RF front end (RF module).

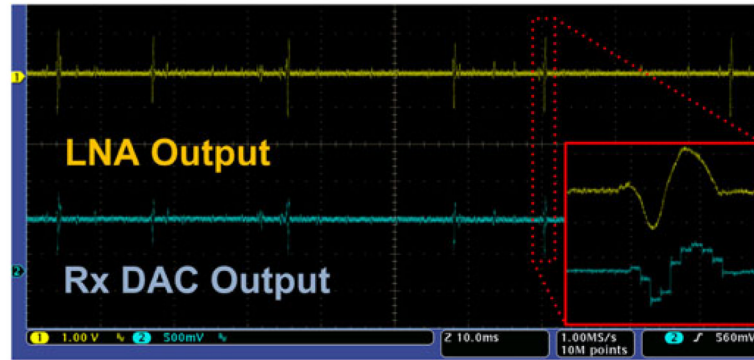


Fig. 8.

Top trace: One of the LNA outputs on the WINeR-6 Tx when a prerecorded neural signal with 1 mV spikes was applied to the input. Bottom trace: DAC output on the WINeR-6 Rx for the same channel at 1.5 m away. Inset: A zoomed-in spike at the Tx and Rx analog outputs.

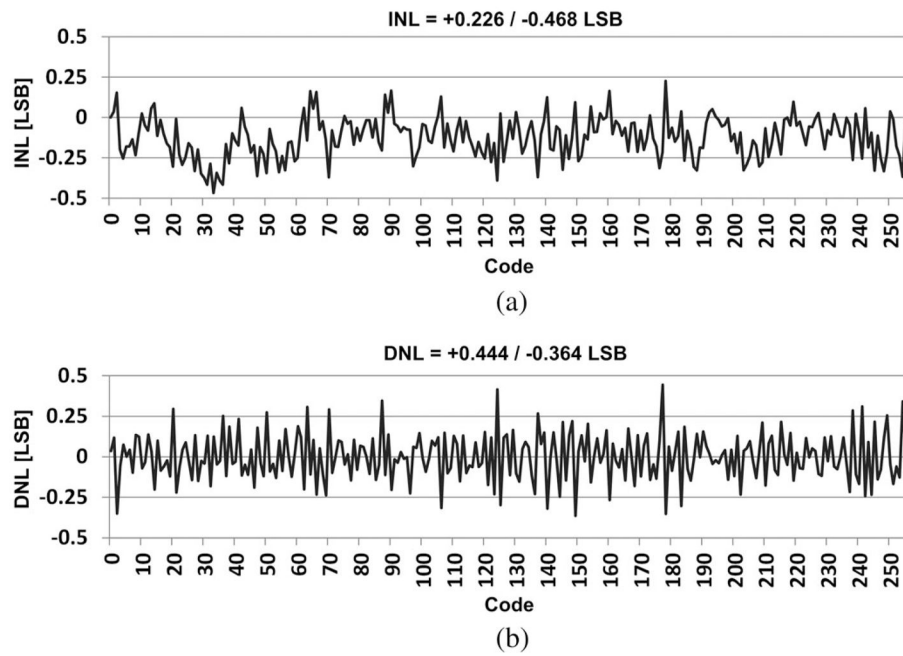
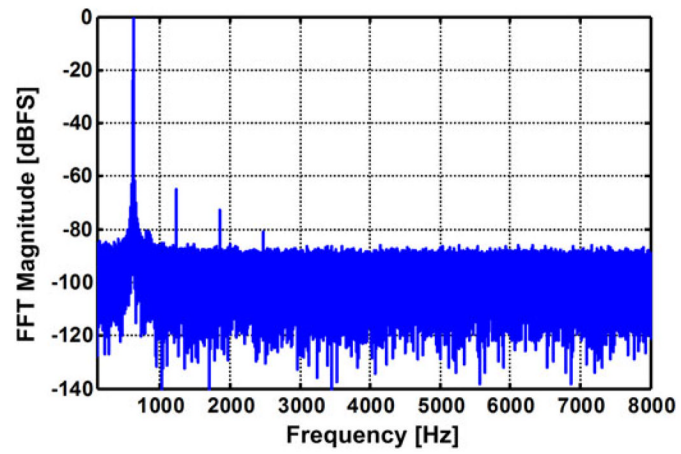
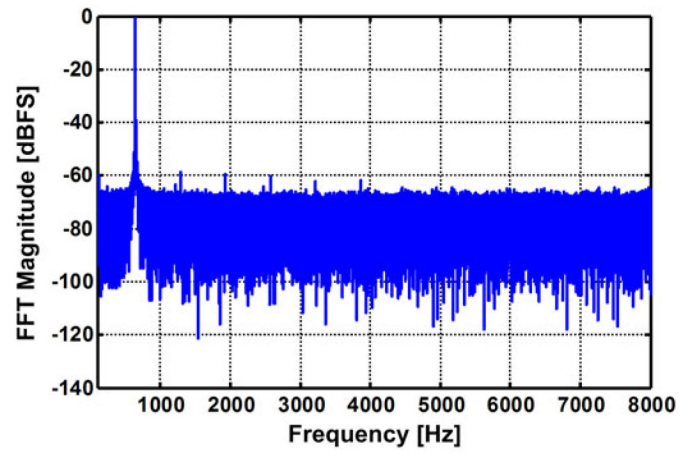


Fig. 9. (a) INL and (b) DNL measurements for the entire WINeR-6 system at the Tx–Rx distance of 150 cm.



(a)



(b)

Fig. 10. Tone test measurements of the WINeR-6 system (a) without wireless link, (b) at the Tx–Rx distance of 150 cm.

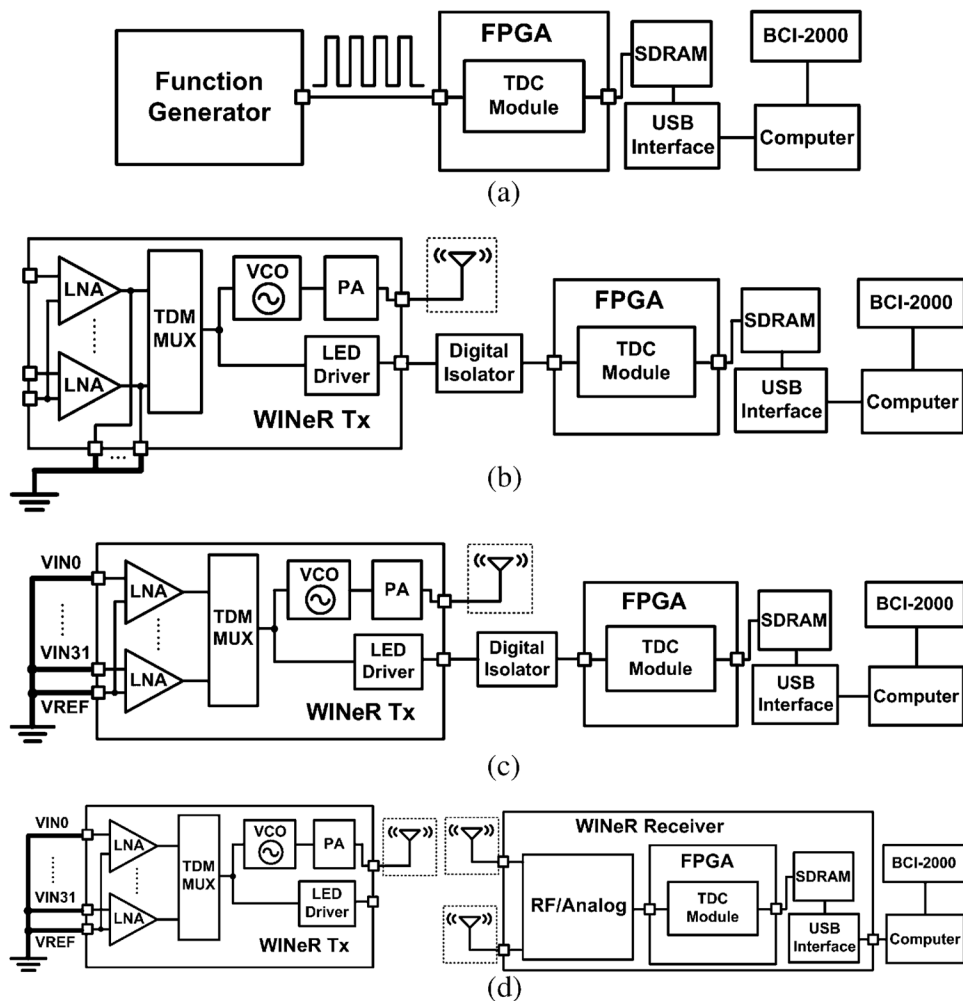


Fig. 11. Various noise measurement configurations to find out the contribution of each major WINEr-6 component to the total system noise: (a) TDC noise measured by connecting a precise function generator, (b) ATC + TDC noise without wireless link, (c) LNA + ATC + TDC noise without wireless link, (d) noise of the entire system.

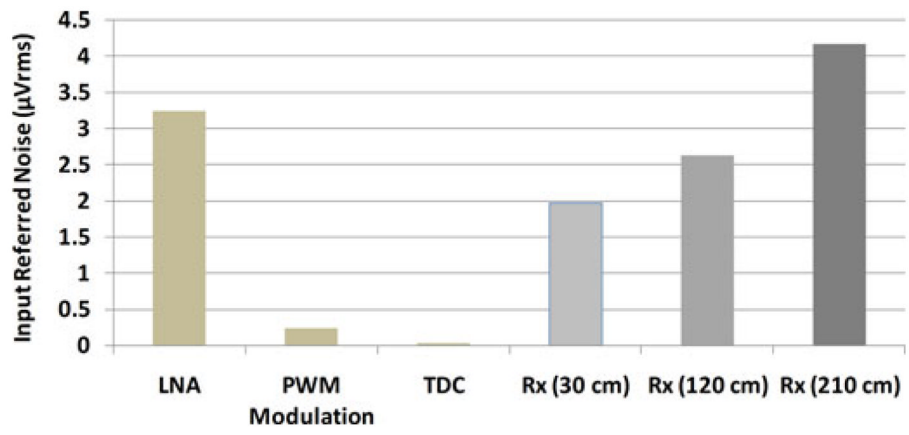


Fig. 12. Noise contributions of different WINEr-6 blocks at 640 kSps.

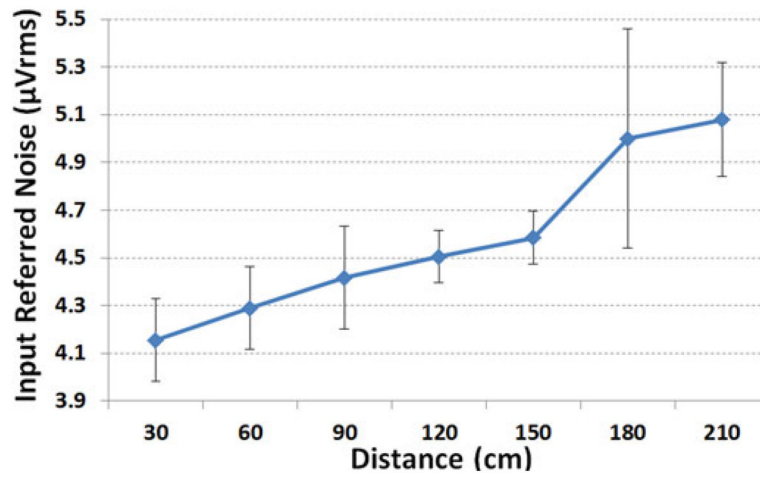


Fig. 13. Noise measurement of the entire WINeR-6 versus Tx-Rx distance.

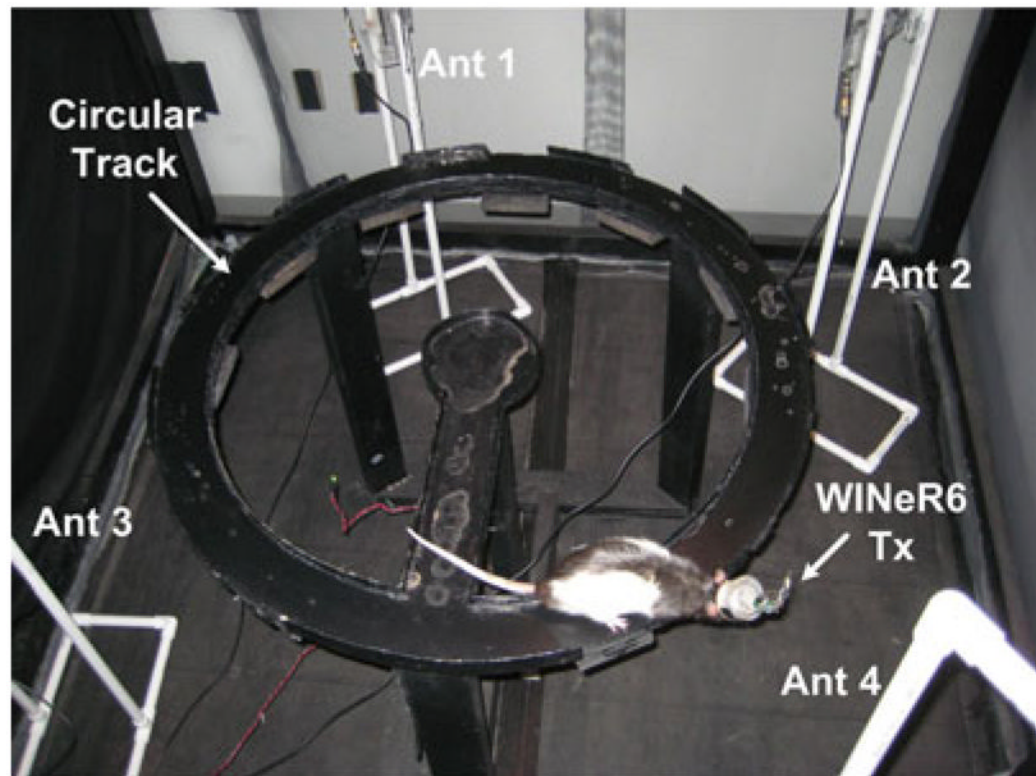


Fig. 14.

Awake freely behaving animal experimental setup. The rat completed two sets of 40 laps on a circular track with ~1 m in outer diameter, while we recorded neural signals simultaneously from 32 channels using WINEr-6 and a hardwired setup. Quality of the recorded neural signals was observed in real time but single unit activities were classified offline and used to construct the place fields in each case after synchronizing and combining the neural activity with the animal position from the recorded video.

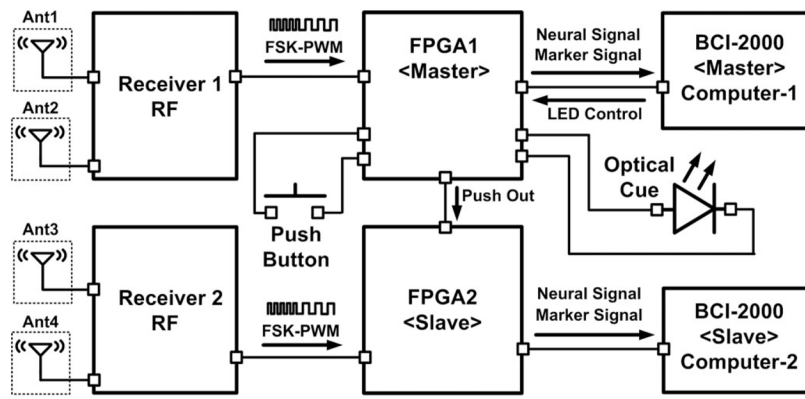


Fig. 15. Synchronization between two WIneR-6 Rxs, each of which has two antennas, with a push button as well as a video stream, using an optical cue.

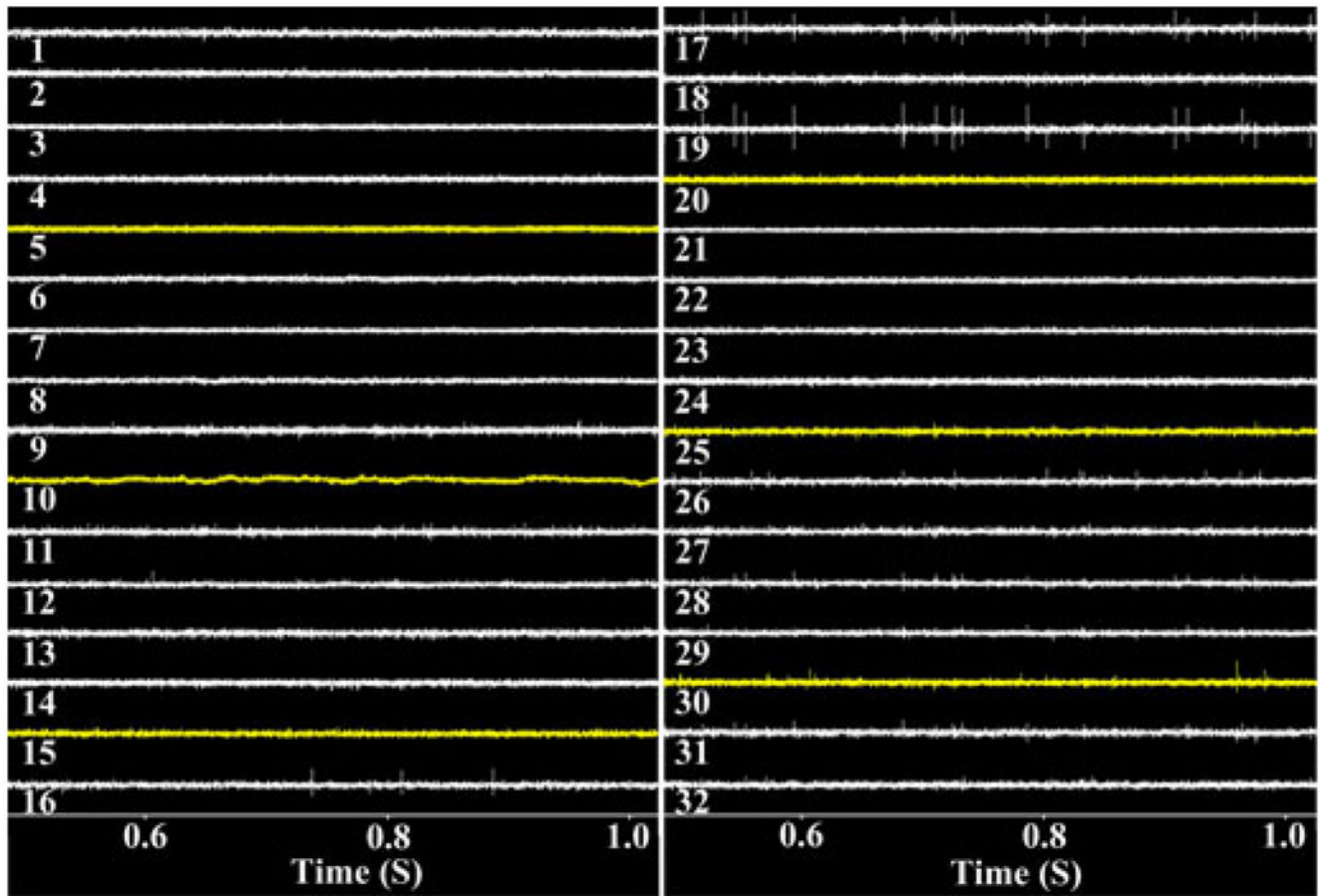
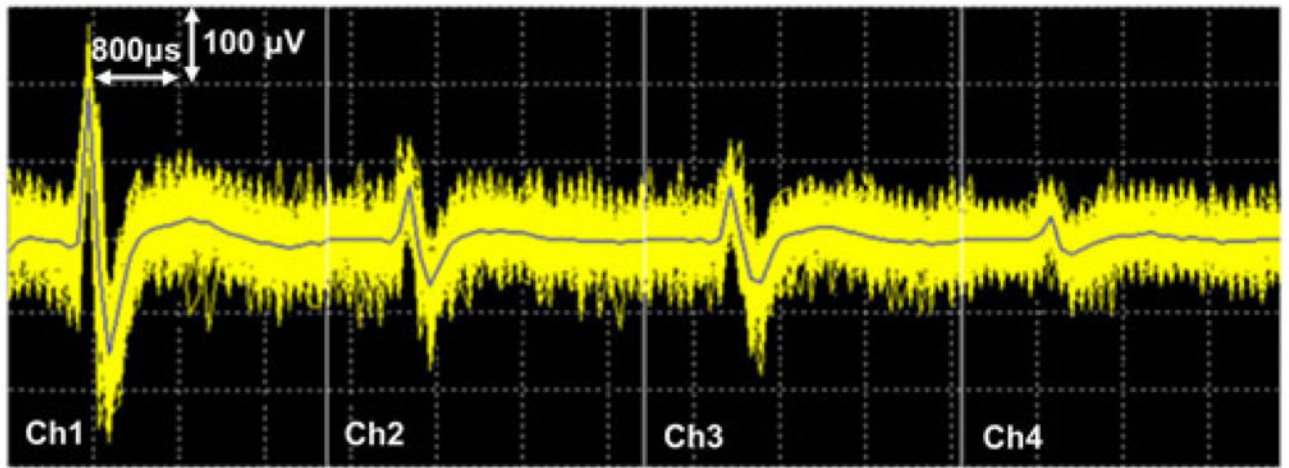
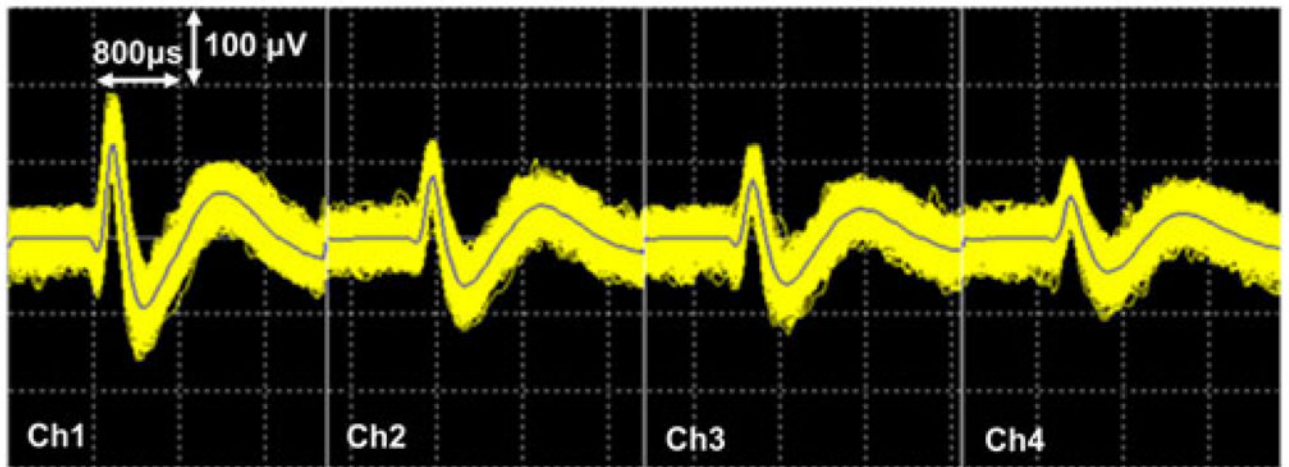


Fig. 16. Time-domain representation of 32-ch recorded signals in real time using the BCI-2000 GUI.



(a)



(b)

Fig. 17. Spike classification of four individual channels in Tetrode 5 from (a) WINEr-6 and (b) NSpike systems using Plexon's Offline Sorter.

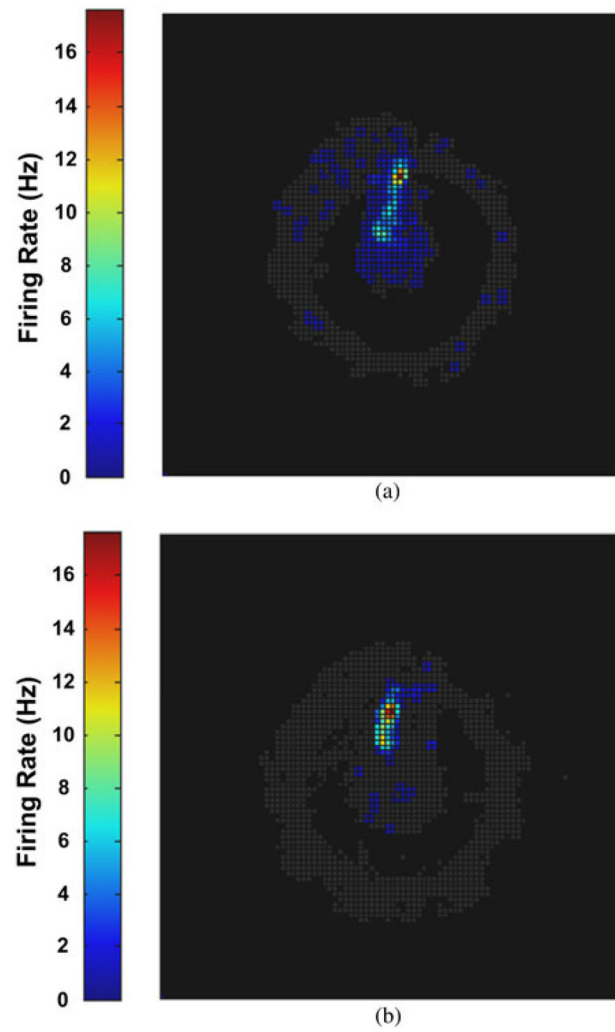


Fig. 18. Comparison between place fields resulted from (a) WINEr-6 wireless and (b) NSpike hardwired recordings.

TABLE I

Summary of the WINeR-6 System Specifications

<i>WINeR-6 Tx ASIC</i> [27]	
Fabrication technology	0.5- μ m Std. CMOS
Number of channels	32 + 4 feedback
Die size (mm ²)	4.93 \times 3.33
Supply voltage (V)	\pm 1.5
Total power consumption at -14 dBm RF output power (mW)	15
Sampling rate from all channels (kSps)	58-709
FSK carrier frequency (MHz)	428/441
<i>WINeR-6 Rx</i>	
Supply voltage (V)	\pm 5
Current consumption (mA)	290 (+5 V), 80 (-5 V)
Size (cm ³)	17.9 \times 17.5 \times 7.6
Bandwidth (MHz)	18
Center frequency (MHz)	433 MHz
Sensitivity (dBm)	-65
Tuning range (MHz)	28(419-447)
Nominal Tx-Rx antenna distance (m)	1.5
Max. Tx-Rx antenna distance (m)	4.2
<i>Neural Recording</i>	
Sampling rate/ch (kSps)	1.6-19.7
LNA gain (dB)	67.8/78
LNA input referred noise (μ V _{rms}) (BW: 200 Hz-8 kHz)	3.25
System input referred noise (μ V _{rms}) (BW: 200 Hz-8 kHz, Distance: 1.5 m)	4.58
System resolution (ENOB)	8
Computer interface	USB 2.0 (480 Mbps Max)
Graphical user interface (GUI)	BCI-2000 (Open source)